Heterogeneous object modeling using signed approximate real distance functions

Pierre-Alain FAYOLLE, Alexander PASKO, Benjamin SCHMITT, Nikolay MIRENKOV

March 11, 2004

Title:

   Heterogeneous object modeling using signed approximate real distance functions

Authors:

   Pierre-Alain FAYOLLE*, Alexander PASKO**, Benjamin SCHMITT***, Nikolay MIRENKOV*

Key Words and Phrases:

   constructive heterogeneous object modeling, distance function approximation, set-theoretic operations, Function Representation (FRep)

Abstract:

   We introduce a smooth approximation of the min/max operations for maintaining an approximate signed distance function in constructive shape modeling. With the use of an additional bounding band for the smooth approximation, we also guarantee a fixed upper bound of the distance function error at any given point.

   In contrast to min/max functions, such a smooth approximation called SARDF (Signed Approximate Real Distance Function) preserves C^1 continuity of the defining function for the resulting object. We apply distance based shape modeling to represent objects with heterogeneous material distribution in the constructive hypervolume model framework. The introduced distance approximation helps intuitively model material distributions parameterized by distances to so-called material features. The lack of smoothness in the material functions could lead to undesirable singularities, for instance, stress concentrations. The C^1 continuity of shape defining functions provides smoothness of the material functions. We illustrate application of the SARDF operations by 2D and 3D heterogeneous object modeling case studies.

Report Date:	Written Language:
3/15/2004	English

Any Other Identifying Information of this Report:

   * The University of Aizu, Aizu Wakamatsu, Japan
   ** University of Hosei, Tokyo, Japan
   *** Computer Graphics Research Institute, Hosei University, Tokyo, Japan

Distribution Statement:

   First Issue: 1 copie

Supplementary Notes:

Contents

1 Introduction

Solid modeling methods have so far focused on developing models of objects for capturing their geometry. Since most of the objects were considered to be homogeneous, such approach was sufficient until now. Recently, particular attention has been paid to modeling heterogeneous objects. In heterogeneous object modeling, an object has a number of non-uniformly distributed attributes assigned at each point and varying in 3D space. Such attributes may or may not be continuous and are of different natures such as photometric, material, physical, and others. Heterogeneous objects are used in different areas such as CAD/CAM, rapid prototyping, physical simulations, geological and medical modeling.

Constructive modeling is based on successively applying set-theoretic and other operations to predefined shapes, called primitives. We provide in this work a new set of functions defining set-theoretic operations to be used in constructive modeling of heterogeneous objects. Such functions provide a controlled approximation of the signed distance function, under the condition that the primitives used in modeling are defined by exact distance functions. They also preserve C^1 continuity of the resulting function. With signed distance functions, one can control and model accurately material distribution in heterogeneous object modeling.

1.1 Previous works

Several techniques to model heterogeneous objects have been proposed during the recent years. Analogies to homogeneous object modeling can be easily noticed. Existing homogeneous object models include surface based boundary representation (BRep), feature based models, or parametric models; and volume based models such as voxel arrays and cellular complexes as discrete representations, or FRep as a continuous representation [PASS95]. Each homogeneous model has been extended for the underlying model to handle heterogeneity. In the following, we propose a brief review of the existing models used in heterogeneous object modeling.

A non-manifold BRep scheme is considered in [KD97]. An object is subdivided in components; each of them is homogeneous inside and has an assigned material index. Set theoretic operations can be applied to the solid's components with the corresponding operations on the material. Unfortunately, such modeling techniques are limited to the representation of discretely varying material properties. In [KBDH99], a more general model is proposed: the geometry is represented by the point set decomposition into a finite set of closed 3-cells, whereas the attributes are defined by a collection of functions mapping the object geometry to several attributes. Such a mathematical model is known as a fiber bundle, with the geometric model playing the role of the base space. Several other works are using the model proposed in [KBDH99], and extend it in various directions ([BSD00, CF03]). Unfortunately, as noticed by [BST02], such model does not offer concrete computational solutions.

Volumetric representations naturally define solids due to their inherent volumetric nature. An homogeneous object is defined as a subset of the 3D space, with an additional scalar value. In the case of a spatial enumeration, in other words in the case of voxels [Req80], extension to heterogeneity consists in adding

a scalar value for each attribute [Nie00]. The drawback of this method is the difficulty to directly describe the material distribution, without the use of a data acquisition device (and therefore it is supposed that the object to be modeled already exists). Furthermore, the discrete property requires some special approximation procedures.

A continuous volumetric representation has been proposed in [QD01], where a B-spline volume is used to model the object geometry, whereas the attributes are modeled by mean of diffusion. This model suffers from the lack of flexibility as the geometry is restricted to volume splines. Other continuous volumetric models exist in the literature, but are related to other areas than CAD/CAM. For instance, in computer graphics, the CVG model, *Constructive Volume Geometry* [CT00], defines an object as a tuple of scalar fields, where the first field of the tuple defines the opacity of the object and determines its geometry, and the other tuples define the object properties, such as photometric, density, temperature properties, and others. This model, initially proposed in the volume graphics area, hardly meets the requirements of the CAD area.

1.2 Problem statement

The above review briefly introduced some of the recent works on heterogeneous object modeling. In most of the proposed techniques, a common terminology can be retrieved. A heterogeneous object is usually composed of different parts, called *features*. Elements of object's geometry are called *geometric features* or *form features*. A *material feature* is a subset of the object's geometry space with known material property. In heterogeneous object modeling, one of the problems is how to model variable material distribution. More generally, given the object's geometry and some material features, how to model, to compute, and to control the distribution functions for different materials.

1.3 Contribution

To solve the above problem, an interesting idea was proposed by [BST02]: the Euclidean space can be parameterized by distance to material features, either exactly or approximately. Functions describing the distance from the given point to material features provide intuitive means for modeling any desired material distributions as they appear in design and manufacturing.

The underlying idea of this proposal is to introduce the use of signed approximate real distance functions in modeling. Object's geometry can be fully described by such functions, i.e., its inside is defined where the distance function takes positive values, its outside is where the distance function is negative, and its boundary as an iso-valued point set, where the distance function usually equals to zero.

After considering the existing works, it appears that the BRep model and its derivatives for heterogeneous object modeling are difficult to extend in a general manner such that they meet the above idea. A more natural solution is to use a model based on a continuous volumetric representation. Unfortunately, this method presents also some drawbacks. Indeed, deriving analytical expressions for a distance function may be a tedious work in the general case. Therefore, the constructive approach would be very helpful in the design of heterogeneous objects.

A general continuous representation of heterogeneous objects, called a *constructive hypervolume model*, was proposed in [PASS01]. In the following subsection, we first present an outline of this model. Then, we propose to restrict this model in order to support distance-based material distributions proposed in [BST02], and finally discuss the problems of this model in the CAD area. Other sections of this document propose solutions to these problems, and illustrate the proposed approach with some case studies.

1.3.1 General constructive hypervolume model

In this paper, we propose to use a distance-based version of the constructive hypervolume model [PASS01] as a mathematical model of heterogeneous objects. In this model, a general hypervolume object is defined as a multidimensional point set G with multiple attributes given at any of its points. The attributes S_i represent abstract values or physical characteristics such as temperature, color, material distribution, etc. In [PASS01], a specific representation of the hypervolume is proposed as:

$$o = (G, A_1, \ldots, A_k) : (F(X), S_1(X), \ldots, S_k(X)) \tag{1}$$

where :

- $X = (x_1, \ldots, x_n)$ is a point in n-dimensional Euclidean space E^n,

- $F : E^n \rightarrow \mathbb{R}$ is a real-valued defining function of point coordinates to represent point sets G, based on the FRep model [PASS95]

- $S_i : SP_i \rightarrow \mathbb{R}$, $SP_i \subset E^n$ is a real-valued scalar function corresponding to an attribute, A_i that is not necessarily continuous.

The function $F(X)$ is a real valued function. For each given point, the function is evaluated and depending on the sign of the returned value, one can classify the given point as inside, outside or on the boundary of the object. This function is represented in the modeling system by a tree structure with primitives in the leaves and operations in the nodes. We generally use the term *constructive tree* for this tree structure. The only requirement of the FRep model is that the defining function F has to be at least C^0 continuous.

Similarly, depending on the applications [SPAS01, AKK$^+$02], the attribute functions can be defined using physical models or the constructive approach. The spatial subset where an attribute is defined, is called a *space partition* designated as SP_i in the above formulation. There are no definite values for an attribute outside its space partition. The relation between a material feature, defined above, and a space partition, can be stated as follows: for each material feature, there is at least one space partition, which contains this material feature. Note that a material feature can be contained in more than one space partition, for example, in the case when the material feature is made of the known composition of several materials.

1.3.2 Distance-based constructive hypervolume model

In some application areas, like computer graphics for instance, the generality of the FRep and of the constructive hypervolume model may be appreciable, but

in some other cases, in particular for CAD and modeling heterogeneous objects with internal material distributions, this model can not be used as it is.

We propose a restriction of this model for handling the particular type of the material distribution based on approximate distance functions [BST02]. Since we need to provide a real signed distance function for the object's geometry, or at least a controlled distance approximation, the primitives are restricted to those, which surface can be defined as a zero level set of the signed distance function (so-called normal primitives). Several primitives are already available including sphere, cylinder, plane, torus, general quadric, block, and ellipsoid [Har96]. This quite strong requirement is needed to accurately compute a signed distance function for constructive solids, and thus correct material distributions for them. Note that a normalization procedure [Rva82], [BS01] can be applied to any defining function of a primitive to approximate the distance near its boundary, but the distance property is not guaranteed far from the boundary, which can be an additional source of the distance error.

In the remaining of this document, we suppose that primitives are defined by signed real valued functions. In order to support the constructive approach to model an object, set-theoretic operations have to be provided.

Let two point sets be defined by $f_1(X) \geq 0$ and $f_2(X) \geq 0$, where f_1 and f_2 are signed real distance functions. Then, the union of these point sets can be defined as $f_3 = max(f_1, f_2)$ and the intersection as $f_3 = min(f_1, f_2)$ [Sab68], [Ric73]. As the functions are signed real distance functions, min/max operations result in the exact distance function for the entire complex object. However, min/max operations have points of C^1 discontinuity by definition. This discontinuity can cause unexpected results at the geometrical level of further operations on the object such as blending, metamorphosis, and others, but also it can have an undesirable influence on the material distribution (stress concentrations, undesirable singularities, see [BST02]).

There are several works on replacing min/max functions in constructive modeling by C^1 continuous exact or approximated descriptions of set-theoretic operations. R-functions [Rva63], [Rva74] provide a distance-like properties of the defining function but not the exact distance function value. Moreover, exponential function value growth can be observed, for example, when applying R-functions to define union of a number of overlapping solids ("positive explosion" effect). In the case of the above mentioned normalized primitives [Rva82], [BS01], the results of R-functions are normalized as well thus keeping the distance approximation near the boundary. The superelliptic min/max approximation [Ric73] does not describe exact set-theoretic operations and suits for blending only. The elliptic min/max approximation [BDS+03], even if applied to normal primitives, can well approximate the distance near the boundary, but the error of the distance function grows infinitely far from the boundary.

We propose here to extend the approach of [BDS+03] for providing approximation of real distance functions by using a circular min/max approximation and by introducing an additional bounding band to guarantee a fixed upper limit of the distance function error at any given point.

As such approximations of min and max functions are acceptable for distance-based modeling, we call the resulting defining functions of shapes by the term signed approximate real distance functions (SARDF), approximate min function can be called "SARDF intersection" and designated as $f_1 \wedge_S f_2$, approximate max function - "SARDF union" designated as $f_1 \vee_S f_2$. Note that SARDF

operations can be applied to both normal and normalized primitives. However, in the latter case the distance property of the resulting function is provided for points located only close to the boundary.

We apply such distance based constructive modeling in the constructive hypervolume model framework [PASS01], with a special attention focused on material distribution. With the help of signed distance approximation, we are able to intuitively model heterogeneous material distributions parameterized by the distance to the material features as suggested in [BST02].

2 SARDF operations

2.1 Overview

Any contour line of the *min* and *max* functions has sharp corner, corresponding to the union of two vertical and horizontal rays. This feature of the contour lines reflects the C^1 discontinuity of the *min* and *max* functions that occurs at any point when two arguments are equal. Figure 1 shows for instance the sharp corners appearing when drawing different contour lines for the *min* function.
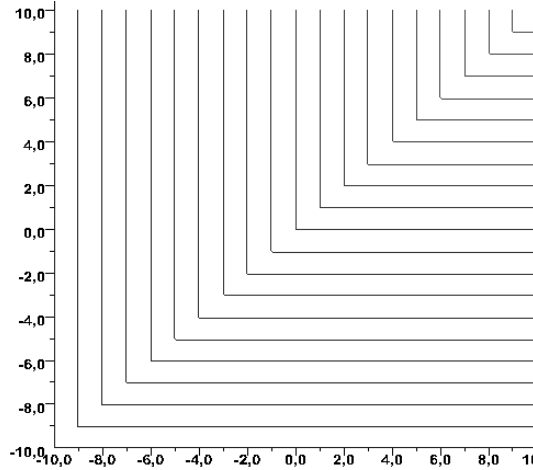

Figure 1: Each contour line of the *min* function contains a sharp corner.

Following the general approach of [BDS+03], we propose to replace the sharp corner in any contour line with a circular arc, as shown in Fig. 2. Two straight lines, symmetric with respect to the line $y = x$, are used to delimit the frontier for the circular arc approximation.
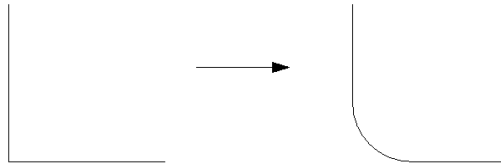

Figure 2: Contour line of the function *min* has a sharp corner (left) to be replaced by a circular arc (right).

The use of the circular approximations for the *min* and *max* functions can provide the C^1 approximation of the resulting distance function for constructive shapes built using normal primitives (defined by distance functions). Unfortunately, this approach has the following problem: the radius of the circular arc used to replace the sharp corners in the contour lines keeps growing with the distance from the initial surfaces. Fig. 3 illustrates this problem for the case of

the *min* function approximation. Because of this behavior of the arc radius, the error of the distance function approximation grows infinitely with the distance, which is unacceptable for distance-based modeling and application algorithms.
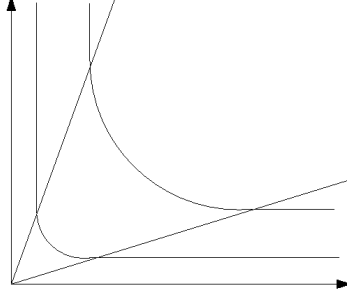

Figure 3: The radius of the circular arc is growing with the distance from the origin, thus increasing the error in the distance function made by the approximation.

We propose to prevent the radius of the circular arc from growing infinitely by introducing a fixed threshold R. A new bounding band can be introduced by two parallel straight lines that enclose the arcs with the fixed radius. These band lines are defined by a shift of the line $y = x$ at R distance in positive and negative x directions: $y = x - R$ and $y = x + R$. They provide for a fixed upper limit of the distance function error at any given point. As such approximations are acceptable for distance based modeling, the resulting defining functions of shapes are called by the term signed approximate real distance functions (SARDF). The union will be called SARDF union and the intersection, SARDF intersection.

All operations are discussed for two half spaces $f_1 = x$, $f_1 \geq 0$ and $f_2 = y$, $f_2 \geq 0$. Later we intend to apply these operations to arbitrary distance functions f_1 and f_2.

The Euclidean plane is divided into four quadrants; the first quadrant corresponds to $x > 0$ and $y > 0$, the second quadrant to $x < 0$ and $y > 0$, the third quadrant to $x < 0$ and $y < 0$, and finally the fourth quadrant to $x > 0$ and $y < 0$. In the second and fourth quadrants, the SARDF union and intersection are equal exactly to *min* and *max*; thus we will restrict the discussion to the first and third quadrants.

In those quadrants, the construction steps for the SARDF union and intersection are very similar, and redundant, therefore we give only details for the case of the SARDF intersection. The complete details for the construction steps of all the SARDF operations, as well as some of their properties, and implementation details, can be found in [FPS03].

2.2 Construction and expression of the SARDF intersection

2.2.1 Quadrant I

The intersections of the two parallel bounding band lines, $y = x + R$ and $y = x - R$, with the lines parallel to the axes, $x = R$ and $y = R$, result in two points: $A_1(2\,R, R)$ and $A_2(R, 2\,R)$, as shown in Fig. 4. These points are connected by the circular arc $(x - 2\,R)^2 + (y - 2\,R)^2 = R^2$. This makes a natural boundary, that splits the first quadrant into two zones I and II, where two approaches for approximation are applied (see Fig. 4).
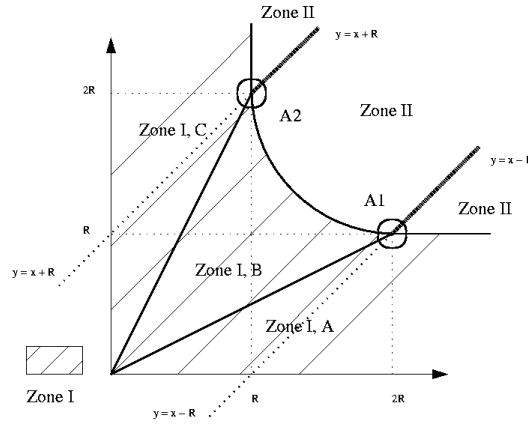

Figure 4: The first quadrant is divided into two zones. The circular approximation is applied in zone I, whereas we introduce a fixed radius approximation with the bounding band in zone II.

Zone I Zone I corresponds to the set of points $P(x, y)$ for which $x < R$ or $y < R$ or $(x < 2\,R$ and $y < 2\,R$ and $(x - 2\,R)^2 + (y - 2\,R)^2 > R^2)$, see Fig. 4.

In this zone, a circular approximation of the function $F(x, y) = min(x, y)$ is used. We want to replace any contour lines $F = d$ with a circular arc and two rays tangentially attached to it as shown in Fig. 5.
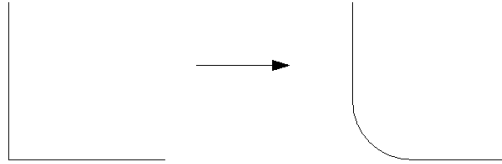

Figure 5: Contour line of the function min has a sharp corner (left) to be replaced by a circular arc (right).

The radius of the circular approximation is growing with the distance to the

9

surface and is bounded by two straight lines L_1 and L_2, symmetric with respect to $y = x$ and defined as follows:

- L_1: $O - A_1$, where O is the origin (0,0),

- L_2: $O - A_2$.

L_1 and L_2 makes an angle α with respectively the x-axis and the y-axis; this angle is defined by $cotan(\alpha) = 2$. These two lines break the zone I of the first quadrant into three new zones: A (below L_1), B (between L_1 and L_2) and C (above L_2), as shown in Fig. 4.

We are interested in the contour lines $\tilde{F} = d$ of the smooth approximation $\tilde{F}$ of the min function. Given an arbitrary point $P(x, y)$, we need to calculate a function value d for it.

In zone A, $\tilde{F}$ is equal to $min(x, y)$, therefore the contour is a horizontal line going through the point P and defined as $\tilde{F} = y$. In zone C, $\tilde{F}$ is also equal to $min(x, y)$, so the contour is a vertical line going through the point P and defined as $\tilde{F} = x$.

Finally, in zone B, we want to have a circular arc passing through the point $P(x, y)$. This arc should go through the point P and change into the horizontal ray in zone A and into the vertical ray in zone C. Both of these rays are at the distance d from the corresponding x and y axes. Such a distance is used for the definition of the value of the function. In order to calculate this distance d, we start from the equation of the circle passing through P:

$$(x - x_0)^2 + (y - y_0)^2 = r^2 \tag{2}$$

In this equation, x_0, y_0 and r are unknown but can be expressed in terms of the value d being searched, and α, the angle between the straight lines and the axes. Fig. 6 shows the unknowns and their geometric relations.
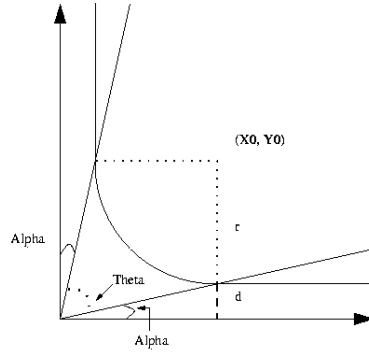

Figure 6: Unknowns of the Eq. 2 and their geometric relations.

In zone A (Fig. 4), from the lower triangle (Fig. 6) the following relation holds: $x_0 = d\,tan(\alpha)$. By analogy, in zone C (Fig. 4) from the upper triangle (Fig. 6) it comes: $y_0 = d\,tan(\alpha)$, and $r = x_0 - d$. By replacing these variables in Eq. 2, we obtain the quadratic equation for the variable d:

$$d^2\,[cotan^2(\alpha) + 2\,cotan(\alpha) - 1] - 2\,d\,(x + y)\,cotan(\alpha) + x^2 + y^2 = 0 \tag{3}$$

The solution of the quadratic Eq. 3 for the unknown d is:

$$d = \begin{cases} \frac{-b \pm (b^2 - 4ac)^{0.5}}{2a} & \text{if } a \neq 0 \text{ and in zone B} \\ -\frac{c}{b} & \text{if } a = 0 \text{ and in zone B} \end{cases}$$

where $a = cotan^2(\alpha) + 2\ cotan(\alpha) - 1$, $b = -2\ (x+y)\ cotan(\alpha)$ and $c = x^2 + y^2$ are the coefficients of the quadratic Eq. 3.

The final expression of the circular approximation $\tilde{F} = d$ for the min function, in the zone I becomes:

$$\tilde{F}(P) = d = \begin{cases} \frac{-b \pm (b^2 - 4ac)^{0.5}}{2a} & \text{if P in zone B} \\ y & \text{if P in zone A} \\ x & \text{if P in zone C} \end{cases}$$

where $a = cotan^2(\alpha) + 2\ cotan(\alpha) - 1 = 7$, $b = -2\ (x+y)\ cotan(\alpha) = -4\ (x+y)$ and $c = x^2 + y^2$.

Zone II In the zone II, the fixed radius with the bounding band is applied to get a smooth approximation $\tilde{F}$ of the min function. Outside the bounding band lines $y = x + R$ and $y = x - R$, the approximation of min is min itself, therefore we take $\tilde{F} = min(x, y)$. Between the lines, we start from the equation of the circle: $(x - x_0)^2 + (y - y_0)^2 = R^2$, where x_0, y_0 are parameters that can be expressed using the radius R and the distance d, which is the searched value of $\tilde{F}$.

Fig. 7 displays these different parameters and their geometric relations. It is obvious that $x_0 = y_0 = d + R$. Replacing x_0 and y_0 in the equation of the circle, the following quadratic expression of the unknown d is obtained: $2\ d^2 + d\ (-2\ x - 2\ y + 4\ R) + (x^2 + y^2 - 2\ x\ R - 2\ y\ R + R^2) = 0$. The solution for the unknown d, gives the searched value for the smooth approximation of the min function: $d = \frac{-b \pm (b^2 - 4ac)^{0.5}}{2a}$, where $a = 2$, $b = -2\ x - 2\ y + 4\ R$ and $c = x^2 + y^2 - 2\ x\ R - 2\ y\ R + R^2$ are the coefficients of the quadratic equation.

The expression for $\tilde{F}$ in the zone II becomes:

$$\tilde{F}(P) = d = \begin{cases} \frac{-b \pm (b^2 - 4ac)^{0.5}}{2a} & \text{inside the bounding band} \\ y & \text{below } y = x - R \\ x & \text{above } y = x + R \end{cases}$$

where $a = 2$, $b = -2\ x - 2\ y + 4\ R$ and $c = x^2 + y^2 - 2\ x\ R - 2\ y\ R + R^2$.

Final expression for the SARDF intersection in the quadrant I We give the final expression for the SARDF intersection $\tilde{F}$ approximating the min function in the first quadrant. Given a point $P(x, y)$ in the first quadrant, the value d of $\tilde{F}$ at P is given by:

$$\tilde{F}(P) = d = \begin{cases} \frac{-b_1 \pm (b_1^2 - 4a_1c_1)^{0.5}}{2a_1} & \text{if P in zone I, B} \\ y & \text{if P in zone I, A} \\ x & \text{if P in zone I, C} \\ \frac{-b_2 \pm (b_2^2 - 4a_2c_2)^{0.5}}{2a_2} & \text{if P in zone II, and inside the bounding band} \\ y & \text{if P in zone II and below } y = x - R \\ x & \text{if P in zone II and above } y = x + R \end{cases}$$
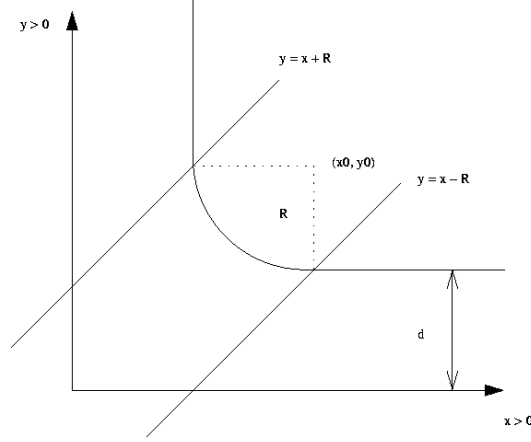
Figure 7: Geometric relations between the parameters of the circular approximation with the bounding band in zone II.

where $a_1 = cotan^2(\alpha) + 2\ cotan(\alpha) - 1 = 7$, $b_1 = -2\ (x+y)\ cotan(\alpha) = -4\ (x+y)$, $c_1 = x^2 + y^2$, $a_2 = 2$, $b_2 = -2\ x - 2\ y + 4\ R$ and $c_2 = x^2 + y^2 - 2\ x\ R - 2\ y\ R + R^2$.

2.2.2 Quadrant III

We consider now the same approach to approximation of the min function with the bounding band in the third quadrant. The intersections of the two parallel bounding band lines, $y = x + R$ and $y = x - R$, with the lines parallel to the axes $x = -R$ and $y = -R$, result in two points: $A_3(-2\ R, -R)$ and $A_4(-R, -2\ R)$, as shown in Fig. 8. These points are connected by the circular arc $(x + R)^2 + (y + R)^2 = R^2$. This makes a natural boundary, that splits the third quadrant into two zones III and IV, for applying the two different approaches to approximation (see Fig. 8).

Zone III   Zone III corresponds to the set of points $P(x, y)$ for which $x > -R$ or $y > -R$ or $(x > -2\ R$ and $y > -2\ R$ and $(x + R)^2 + (y + R)^2 < R^2)$, see Fig. 8. In this zone, the same circular approximation as in zone I is applied. The continuation of the two straight lines L_1 and L_2 into the zone III, breaks it into three more zones: D above L_1, E between L_1 and L_2, and F below L_2 as indicated in Fig. 8.

Given an arbitrary point $P(x, y)$ in the third quadrant, we want to evaluate $\tilde{F}$, the smooth approximation of the min function at this point.

In zone D, $\tilde{F}$ is equal to $min(x, y)$, therefore the contour is a vertical line going through the point P and defined as $\tilde{F} = x$. In zone F, $\tilde{F}$ is also equal to $min(x, y)$, so the contour is a horizontal line going through the point P and defined as $\tilde{F} = y$.

In zone E, we want to have a circular arc passing through the point $P(x, y)$. This arc should go through the point P and change into the horizontal ray in zone F and into the vertical ray in zone D. Both of these rays are at the distance
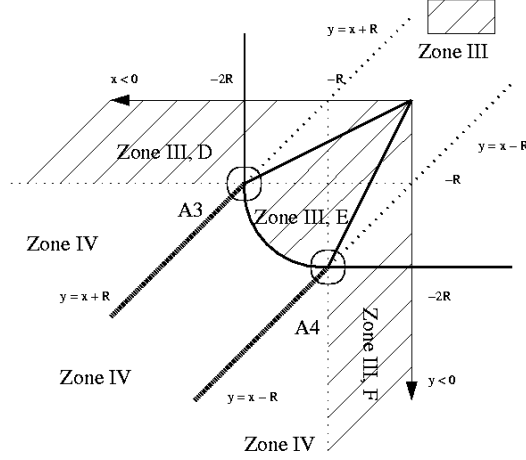
Figure 8: The third quadrant is divided into two zones. The circular approximation is applied in zone III, whereas we introduce a fixed radius approximation with the bounding band in zone IV.

d from the corresponding x and y axes. Such a distance is used for the definition of the value of the function.

Again, in order to calculate this distance d, we start from the equation of the circle passing through P:

$$(x - x_0)^2 + (y - y_0)^2 = r^2 \tag{4}$$

In this equation, x_0, y_0 and r are unknown but can be expressed in terms of d and angle α. Fig. 9 shows the unknowns and their geometric relations.

From the triangle in zone D, $y_0 = -d\ tan(\alpha)$. By analogy, from the triangle in zone F, $x_0 = -d\ tan(\alpha)$, and $d = r + |x_0|$. By replacing these variables in Eq. 4, we obtain the quadratic equation for the variable d:

$$d^2 \left[tan^2(\alpha) + 2\ tan(\alpha) - 1\right] + 2\ d\ (x + y)\ tan(\alpha) + x^2 + y^2 = 0 \tag{5}$$

The solution of the quadratic Eq. 5 for the unknown d is:

$$d = \begin{cases} -\frac{-b \pm (b^2 - 4ac)^{0.5}}{2a} & \text{if } a \neq 0 \text{ and P in zone E} \\ \frac{c}{b} & \text{if } a = 0 \text{ and P in zone E} \end{cases}$$

where $a = tan^2(\alpha) + 2\ tan(\alpha) - 1$, $b = 2\ (x + y)\ tan(\alpha)$ and $c = x^2 + y^2$ are the coefficients of the quadratic Eq. 5. This solution d gives the value for $\tilde{F}$, at P.

The final expression of the smooth approximation $\tilde{F} = d$ for the *min* function, in the zone III becomes:

$$\tilde{F}(P) = d = \begin{cases} -\frac{-b \pm (b^2 - 4ac)^{0.5}}{2a} & \text{if P in zone E} \\ y & \text{if P in zone F} \\ x & \text{if P in zone D} \end{cases}$$

where $a = tan^2(\alpha) + 2\ tan(\alpha) - 1 = \frac{1}{4}$, $b = 2\ (x + y)\ tan(\alpha) = (x + y)$ and $c = x^2 + y^2$.
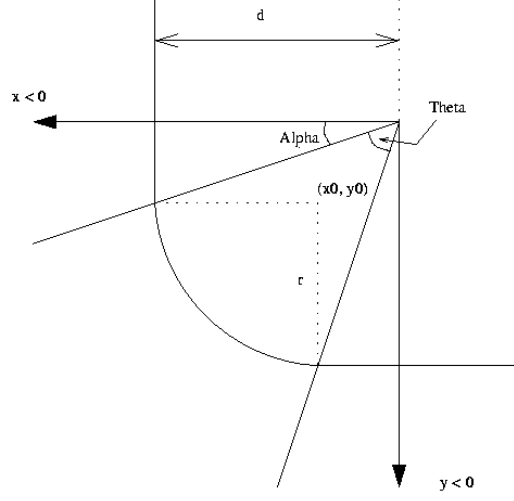
Figure 9: Unknowns of the Eq. 4 and their geometric relations.

Zone IV In zone IV, we switch to a fixed radius approximation with the bounding band. Outside the bounding band, we take $\tilde{F} = min(x, y)$. Inside the bounding band, we start from the equation of the circle: $(x - x_0)^2 + (y - y_0)^2 = R^2$, where x_0, y_0 are parameters that can be expressed using the radius R and the distance d, which is the searched value of $\tilde{F}$.

Fig. 10 shows these different parameters and their geometric relations. It is obvious that $|x_0| = |y_0| = d + R$. Replacing x_0 and y_0 in the equation of the circle, the following quadratic expression of the unknown d is obtained: $2d^2 + d \ (2 \ x + 2 \ y - 4 \ R) + (x^2 + y^2 - 2 \ x \ R - 2 \ y \ R + R^2) = 0$. The solution for the unknown d gives the value $d = -\frac{-b \pm (b^2 - 4ac)^{0.5}}{2a}$, where $a = 2$, $b = 2 \ x + 2 \ y - 4 \ R$ and $c = x^2 + y^2 - 2 \ x \ R - 2 \ y \ R + R^2$ are the coefficients of the quadratic equation.
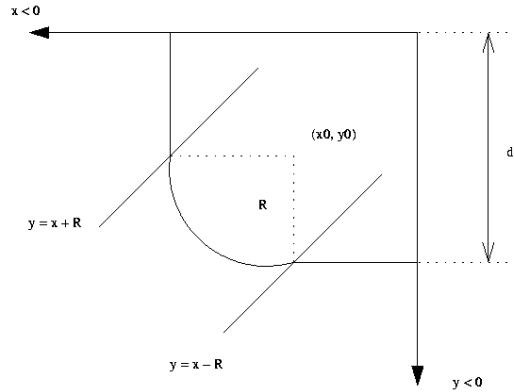

Figure 10: Geometric relations between the parameters of the circular approximation with the bounding band in zone IV.

The expression for $\tilde{F}$ in zone IV becomes:

$$\tilde{F}(P) = d = \begin{cases} -\frac{-b\pm(b^2-4ac)^{0.5}}{2a} & \text{inside the bounding band} \\ y & \text{below } y = x - R \\ x & \text{above } y = x + R \end{cases}$$

where $a = 2$, $b = 2\,x + 2\,y - 4\,R$ and $c = x^2 + y^2 - 2\,x\,R - 2\,y\,R + R^2$.

Final expression for the SARDF intersection in the quadrant III We give the final expression for the SARDF intersection $\tilde{F}$ approximating the min function in the third quadrant. Given a point $P(x, y)$ in the third quadrant, the value d of $\tilde{F}$ at P is defined as:

$$\tilde{F}(P) = d = \begin{cases} -\frac{-b_1\pm(b_1^2-4a_1c_1)^{0.5}}{2a_1} & \text{if P in zone III, E} \\ y & \text{if P in zone III, F} \\ x & \text{if P in zone III, D} \\ -\frac{-b_2\pm(b_2^2-4a_2c_2)^{0.5}}{2a_2} & \text{if P in zone IV, and inside the bounding band} \\ y & \text{if P in zone IV and below } y = x - R \\ x & \text{if P in zone IV and above } y = x + R \end{cases}$$

where $a_1 = tan^2(\alpha) + 2\,tan(\alpha) - 1 = \frac{1}{4}$, $b_1 = 2\,(x+y)\,tan(\alpha) = (x+y)$, $c_1 = x^2 + y^2$, $a_2 = 2$, $b_2 = 2\,x + 2\,y - 4\,R$ and $c_2 = x^2 + y^2 - 2\,x\,R - 2\,y\,R + R^2$.

2.2.3 SARDF intersection of arbitrary objects

In the general case, x and y in the proposed approach can be replaced by the distance functions f_1 and f_2 of two arbitrary FRep objects. Then the intersection between these two objects can be described by the SARDF intersection function as follows:

Case 1: $f_1 > 0$ and $f_2 > 0$ In the current paragraph, E_1 is used for the following boolean expression: $E_1 = (f_1 < R$ or $f_2 < R$ or $(f_1 < 2\,R$ and $f_2 < 2\,R$ and $(f_1 - 2\,R)^2 + (f_2 - 2\,R)^2 > R^2))$.

$$f_1 \wedge_S f_2 = \tilde{F}(f_1, f_2) = \begin{cases} \frac{-b_1\pm(b_1^2-4a_1c_1)^{0.5}}{2a_1} & \text{if } E_1 \text{ and } \frac{1}{2} < \frac{f_2}{f_1} < 2 \\ f_2 & \text{if } E_1 \text{ and } \frac{f_2}{f_1} \leq \frac{1}{2} \\ f_1 & \text{if } E_1 \text{ and } \frac{f_2}{f_1} \geq 2 \\ \frac{-b_2\pm(b_2^2-4a_2c_2)^{0.5}}{2a_2} & \text{if } !E_1 \text{ and } f_1 - R < f_2 < f_1 + R \\ f_2 & \text{if } !E_1 \text{ and } f_2 \leq f_1 - R \\ f_1 & \text{if } !E_1 \text{ and } f_2 \geq f_1 + R \end{cases}$$

where $a_1 = cotan^2(\alpha) + 2\,cotan(\alpha) - 1 = 7$, $b_1 = -2\,(f_1 + f_2)\,cotan(\alpha) = -4\,(f_1 + f_2)$, $c_1 = f_1{}^2 + f_2{}^2$, $a_2 = 2$, $b_2 = -2\,f_1 - 2\,f_2 + 4\,R$ and $c_2 = f_1{}^2 + f_2{}^2 - 2\,f_1\,R - 2\,f_2\,R + R^2$.

Case 2: $f_1 \leq 0$ and $f_2 \geq 0$

$$f_1 \wedge_S f_2 = \tilde{F}(f_1, f_2) = f_1$$

Case 3: $f_1 < 0$ **and** $f_2 < 0$ We denote by E_2 the following boolean expression: $E_2 = (f_1 > -R$ or $f_2 > -R$ or $(f_1 > -2\ R$ and $f_2 > -2\ R$ and $(f_1 + R)^2 + (f_2 + R)^2 < R^2))$.

$$f_1 \wedge_S f_2 = \tilde{F}(f_1, f_2) = \begin{cases} -\frac{-b_1 \pm (b_1^2 - 4a_1 c_1)^{0.5}}{2a_1} & \text{if } E_2 \text{ and } \frac{1}{2} < \frac{f_2}{f_1} < 2 \\ f_2 & \text{if } E_2 \text{ and } \frac{f_2}{f_1} \leq \frac{1}{2} \\ f_1 & \text{if } E_2 \text{ and } \frac{f_2}{f_1} \geq 2 \\ -\frac{-b_2 \pm (b_2^2 - 4a_2 c_2)^{0.5}}{2a_2} & \text{if } !E_2 \text{ and } f_1 - R \leq f_2 \leq f_1 + R \\ f_2 & \text{if } !E_2 \text{ and } f_2 < f_1 - R \\ f_1 & \text{if } !E_2 \text{ and } f_2 > f_1 + R \end{cases}$$

where $a_1 = tan^2(\alpha) + 2\ tan(\alpha) - 1 = \frac{1}{4}$, $b_1 = 2\ (x + y)\ tan(\alpha) = (x + y)$, $c_1 = x^2 + y^2$, $a_2 = 2$, $b_2 = 2\ x + 2\ y - 4\ R$ and $c_2 = x^2 + y^2 - 2\ x\ R - 2\ y\ R + R^2$.

Case 4: $f_1 \geq 0$ **and** $f_2 \leq 0$

$$f_1 \wedge_S f_2 = \tilde{F}(f_1, f_2) = f_2$$

2.3   SARDF union of arbitrary objects

For reasons of symmetry, the construction of the SARDF union in the quadrants I and III, is almost the same as for the SARDF intersection. Therefore, details are skipped and only the final expressions of the union of two arbitrary FRep objects are given.

Case 1: $f_1 > 0$ **and** $f_2 > 0$ In the current paragraph, E_3 is used for the following boolean expression: $E_3 = (f_1 < R$ or $f_2 < R$ or $(f_1 < 2\ R$ and $f_2 < 2\ R$ and $(f_1 - R)^2 + (f_2 - R)^2 < R^2))$.

$$f_1 \vee_S f_2 = \begin{cases} \frac{-b_1 \pm (b_1^2 - 4a_1 c_1)^{0.5}}{2a_1} & \text{if } E_3 \text{ and } \frac{1}{2} < \frac{f_2}{f_1} < 2 \\ f_1 & \text{if } E_3 \text{ and } \frac{f_2}{f_1} \leq \frac{1}{2} \\ f_2 & \text{if } E_3 \text{ and } \frac{f_2}{f_1} \geq 2 \\ \frac{-b_2 \pm (b_2^2 - 4a_2 c_2)^{0.5}}{2a_2} & \text{if } !E_3 \text{ and } f_1 - R < f_2 < f_1 + R \\ f_1 & \text{if } !E_3 \text{ and } f_2 \leq f_1 - R \\ f_2 & \text{if } !E_3 \text{ and } f_2 \geq f_1 + R \end{cases}$$

where $a_1 = tan^2(\alpha) + 2\ tan(\alpha) - 1 = \frac{1}{4}$, $b_1 = -2\ (f_1 + f_2)\ tan(\alpha) = -(f_1 + f_2)$, $c_1 = f_1^2 + f_2^2$, $a_2 = 2$, $b_2 = -2\ f_1 - 2\ f_2 - 4\ R$ and $c_2 = f_1^2 + f_2^2 + 2\ f_1\ R + 2\ f_2\ R + R^2$.

Case 2: $f_1 \leq 0$ **and** $f_2 \geq 0$

$$f_1 \vee_S f_2 = f_2$$

Case 3: $f_1 < 0$ **and** $f_2 < 0$ We denote by E_4 the following boolean expression: $E_4 = (f_1 > -R$ or $f_2 > -R$ or $(f_1 > -2\ R$ and $f_2 > -2\ R$ and $(f_1 + 2\ R)^2 +$

$(f_2 + 2\ R)^2 > R^2))$.

$$f_1 \vee_S f_2 = \begin{cases} -\frac{-b_1 \pm (b_1^2 - 4a_1 c_1)^{0.5}}{2a_1} & \text{if } \frac{1}{2} < \frac{f_2}{f_1} < 2 \text{ and } E_4 \\ f_2 & \text{if } E_4 \text{ and } \frac{f_2}{f_1} \leq \frac{1}{2} \\ f_1 & \text{if } E_4 \text{ and } \frac{f_2}{f_1} \geq 2 \\ -\frac{-b_2 \pm (b_2^2 - 4a_2 c_2)^{0.5}}{2a_2} & \text{if } !E_4 \text{ and } f_1 - R \leq f_2 \leq f_1 + R \\ f_2 & \text{if } !E_4 \text{ and } f_2 < f_1 - R \\ f_1 & \text{if } !E_4 \text{ and } f_2 > f_1 + R \end{cases}$$

where $a_1 = cotan^2(\alpha) + 2\ cotan(\alpha) - 1 = 7$, $b_1 = 2\ (f_1 + f_2)\ cotan(\alpha) = 4\ (f_1 + f_2)$, $c_1 = f_1^2 + f_2^2$, $a_2 = 2$, $b_2 = 2\ f_1 + 2\ f_2 - 4\ R$ and $c_2 = f_1^2 + f_2^2 + 2\ f_1\ R + 2\ f_2\ R + R^2$.

Case 4: $f_1 \geq 0$ **and** $f_2 \leq 0$

$$f_1 \vee_S f_2 = f_1$$

3   Estimation of the distance error for SARDF operations

3.1   Upper limit of the distance error for a single SARDF operation

The upper limit of the distance error for a single SARDF operation is reached in the band area, where the traditional operation (min/max) is replaced by an arc of circle of fixed radius R. For reason of symmetry, the upper limit error for the SARDF intersection and union is the same in absolute value in all the quadrants, so only one case needs to be studied. Let us consider the SARDF intersection in the first quadrant. Fig. 11 reminds the configuration of the first quadrant, with the smooth approximation and the different zones.

The error made at one given point (x, y), when using the SARDF intersection instead of the min itself in the circular shape area (it can be both in the Zone I,B or in the zone II) is shown in Fig. 12a. Let (x, y) be one point for which the distance approximation to the intersection of the two half-planes $x \geq 0$ and $y \geq 0$ is computed. Outside the angle zone used for the circular approximation (zone I,B in Fig. 11) and outside the bounding band (zone II, in Fig. 11), the error is 0. An error is introduced only in the zones of the smooth approximation: zone I,B and zone II (Fig. 11). One upper limit error can be computed in the zone II, inside the band. Fig. 12b shows this area, with the distance error at different points in dashed line. The upper limit for the distance error is reached at the point P defined by $x = y$.

For that particular point, the error is exactly $\epsilon = y = x$; $P(x, y)$ being a point of the circular arc shape of radius R, its coordinates follow the equation: $(x - R)^2 + (y - R)^2 = R^2$. Since $x = y$, it follows that: $2\ x^2 - 4\ Rx + R^2 = 0$, for which the two solutions can be easily obtained. One of this solution can be discarded, since it does not respect the condition $x \leq R$, therefore only $x = \frac{(\sqrt{2}-1)}{\sqrt{2}}R$ remains. This value is an upper bound for the distance error made when using SARDF.
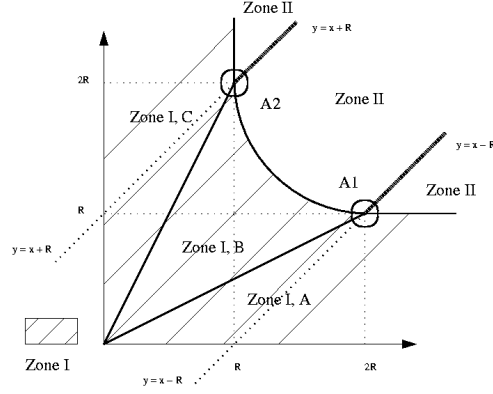
Figure 11: The first quadrant is divided into two zones. The circular approximation is applied in zone I, whereas we introduce a fixed radius approximation with the bounding band in zone II.
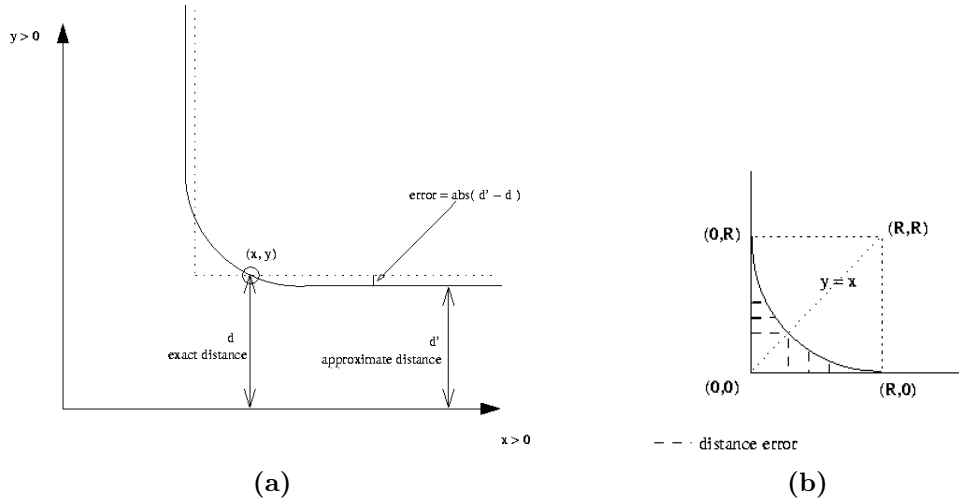

Figure 12: (a) Exact distance, computed approximate distance and error at a given point (x, y). (b) Distance error (in dashed lines) at different points in the band zone (zone II), and max error reached for $x = y$.

18

In the case of the SARDF union operator, the absolute value of the error should be subtracted to the computed approximate distance, in order to have the correct distance value; whereas in the case of the SARDF intersection operator, the absolute value of the error needs to be added to the computed approximate distance in order to get the correct distance value.

3.2 Algorithm for the exact distance error evaluation

The distance error can be evaluated exactly at any point with the following steps:

1. Evaluate the approximate distance using SARDF operations in the constructive tree nodes;

2. Replace in the constructive tree all the occurrences of the SARDF intersection and union, by min and max functions;

3. Evaluate the exact distance function by traversing the tree with the replaced nodes;

4. The distance error is the difference between the two above computed values.

Note that the distance error can be zero depending on the given point position and the operations applied in the construction.

4 Comparison of time efficiency between SARDF and the min/max operations

Because the SARDF intersection and union are more complicated than the min and max functions, they require more time for their execution. Therefore, we looked at their time efficiency and checked that the overhead in time, compared to the min/max functions but also to the R-Function intersection and union, remains reasonable and does not forbid a practical use of these functions.

Subdivisions	Time (in sec.)					
	SARDF intersection	min	R-Function intersection	SARDF union	max	R-Function union
$1001 * 1001$	0.05	0.01	0.02	0.05	0.01	0.02
$10001 * 10001$	5.29	1.42	2.52	4.97	1.38	2.56
$20001 * 20001$	21.18	5.65	10.09	19.59	5.53	10.07
$30001 * 30001$	47.47	12.66	22.75	44.07	12.46	22.72

Table 1: Time efficiency for 1001*1001, 10001*10001, 20001*20001 and 30001*30001 evaluations of SARDF intersection, SARDF union, min, max, R-Function for the intersection and R-Function for the union.

In order to measure the time efficiency, a square was considered in the $x - y$ plane, starting from $(-10, -10)$ and going to $(10, 10)$; this square is regularly subdivided along the x and y axis; let n_x and n_y be the number of subdivisions

along the x and y axis respectively. Then, for each of the functions, the time taken for evaluating these $n_x \times n_y$ points in the square is considered. The results of these evaluations for different subdivisions and all the functions (SARDF intersection and union, min and max, R-Function intersection and union) is given in Table 1.

The overhead in time between the SARDF intersection, min and the R-Function intersection in one hand, and between the SARDF union, max and the R-Function intersection in the other hand are shown in Fig. 13a and b respectively. In our test, we found a factor of approximately 4 between the SARDF operations and the traditional min/max, and a factor of approximately 2 between the SARDF operations and the R-Function.

All the functions considered in the tests were implemented in ANSI C and compiled with the optimization flags turned on, the time results were obtained on a Pentium 4 processor, with 256 MBytes of RAM.
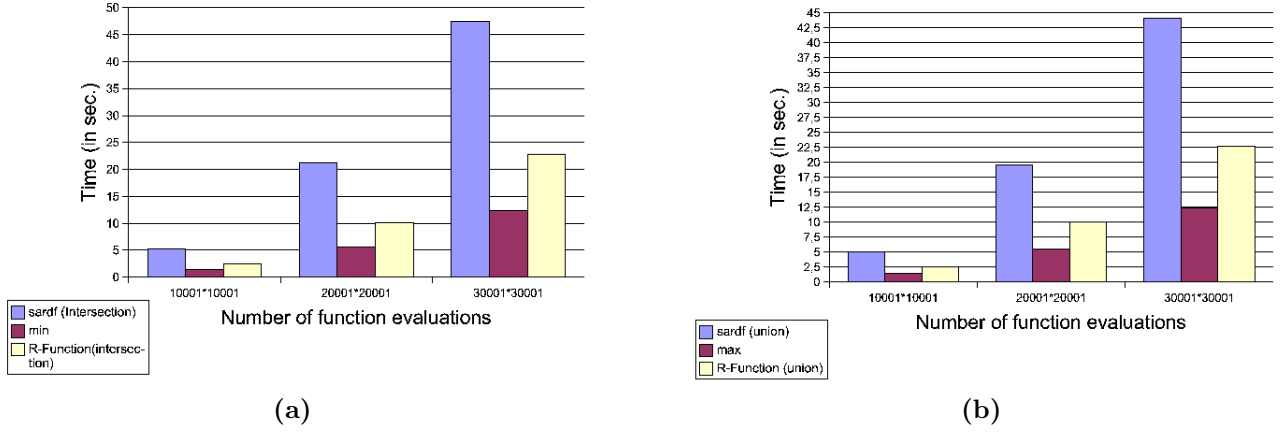

(a)   (b)

Figure 13: Time comparison between: (a) SARDF intersection, min, and R-Intersection; (b) SARDF union, max, and R-Union for different number of function evaluations.

5 Comparison of different union operations: SARDF union, max, and R-union

In the following discussion, the same object, an union of ellipsoids, is modeled with three different union operations, in order to highlight their differences. We are interested in the distance properties and in the C^1 continuity. The considered union operations are: the SARDF union, described above, the max operations [Ric73], and the R-union [Rva63, Rva74, Rva82]. The expression for the SARDF union operation is given in section **??** and we remind for commodity the expression of the R-union of two objects defined by their FRep f_1 and f_2: $f_1 \vee f_2 = f_1 + f_2 + \sqrt{f_1^2 + f_2^2}$. The procedure used for computing the exact signed distance from a point in $\mathbb{R}^3$ to the surface of the ellipsoid can be found in [Har94].

The considered geometric model is the union of two ellipsoids, the first one centered in $(5, 0, 0)$, with radii $(5, 2, 2)$, and the second one centered in $(5, 0, -5)$, with radii $(2, 2, 5)$. For rendering, cross-sections by the plane $y = 0$ are done, see Fig. 14 and 15.

Figures 14a, b, and c, show the interior contour lines of the distance function (positive values of the function) for the whole geometric object. Figure 14a corresponds to the model made with SARDF union, Fig. 14b with the one made with max union, and Fig. 14c with the one made with R-Function. One can notice in Fig. 14c how the use of R-functions results in wrong distance values. In contrary, Figs. 14a and b show very similar contour lines, except at the points joining the contour lines of the two functions, which are smoothed. This artifact is even more visible in Fig. 14d and e, where a zoom is performed on one of the critical area. Figure 14f is a zoom to the model obtained with R-Function and shows that the contour lines are even smoother, but the computed distance to the surface is incorrect.

Some "sharp features" of contour lines can be seen on the main axis of the ellipsoid in Fig. 14a and b. They correspond to points of C^1 discontinuity for the function returning the distance to an ellipsoid. Indeed, it is known that exact distance functions can be C^1 discontinuous on some surfaces, curves or points in 3D space. It is a property of exact distance function without any consideration of how it is obtained. In fact, as soon as two points of the shape have an equal distance to the given point in space, the distance function is C^1 discontinuous at this point. The medial axis corresponds to this set of points of the distance function C^1 discontinuity for the given shape. Applying min and max operations is one of the ways of constructing distance functions, but these operations result in C^1 discontinuity of the defining function at internal and external points of the object. The proposed SARDF operations provide a way to avoid this discontinuity, in constructive modeling, but if a primitive has its own discontinuity on its medial axis, we cannot do anything yet about it. This is a source of future work.

Figure 15 shows the contour lines outside the ellipsoid (negative values of the function) with the different union operations used in the constructive modeling process. Again the use of R-Functions results in a wrong computed distance, especially when going far from the surface of the ellipsoid (see Fig. 15c). When max is used for the union, see Fig. 15b, the distance returned is correct, but sharp points appear, corresponding to C^1 discontinuities in the function defining
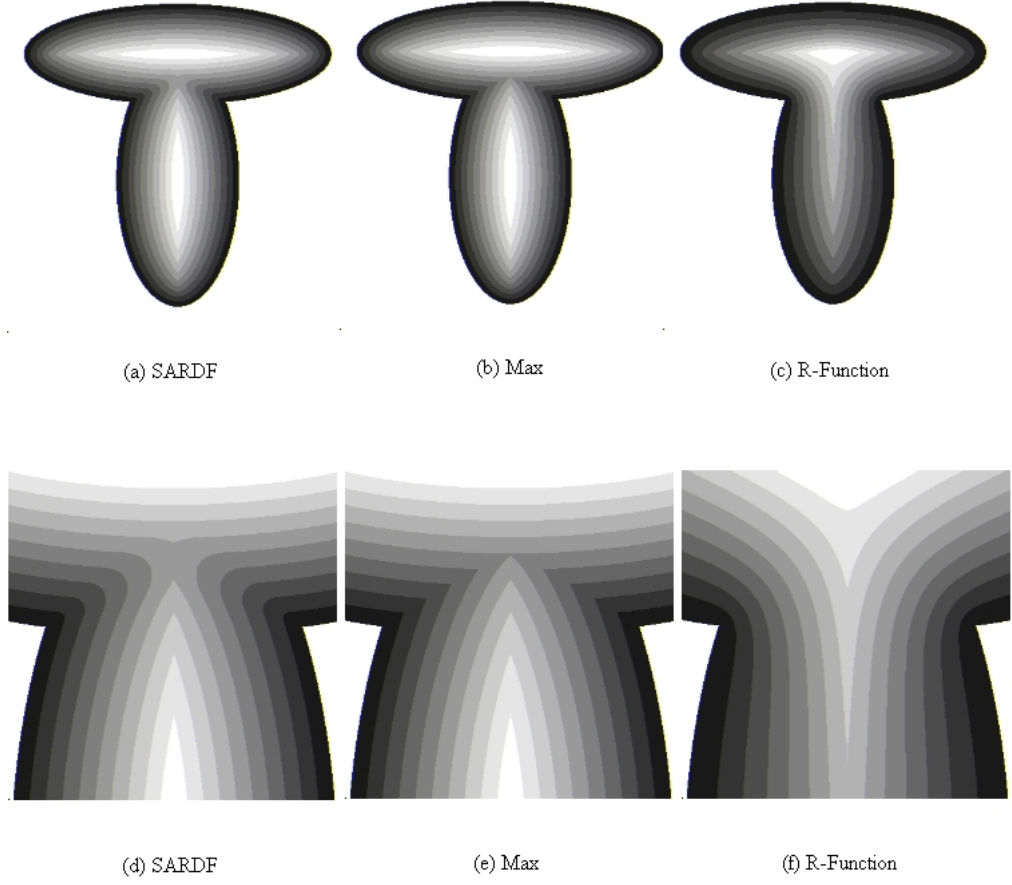
Figure 14: Union of two ellipsoids with different union operations. The level of gray corresponds to range of distances from points inside the ellipsoid to its surface. (a) SARDF union is used, (b) max is used, (c) R-union is used. At the bottom, a zoom is performed to show the behavior of the contour lines in the zone of union: (d) SARDF union is used, (e) max is used, (f) R-union is used.

the solid.

6 Case studies

We propose case studies of constructive heterogeneous modeling with signed approximate distance functions, using SARDF operations and normal primitives.

The SARDF operations are used instead of the R-functions or the min, max operations in the different constructive trees, i.e. for the geometry and the attributes. By a normal primitive, we mean a primitive with a defining function p, which at a given point $x \in \mathbb{R}^3$, returns the Euclidean distance from x to the surface $p^{-1}(0)$. A list of the existing primitives, with the distance function property, can be found in [Har96]. The use of signed distance approximation
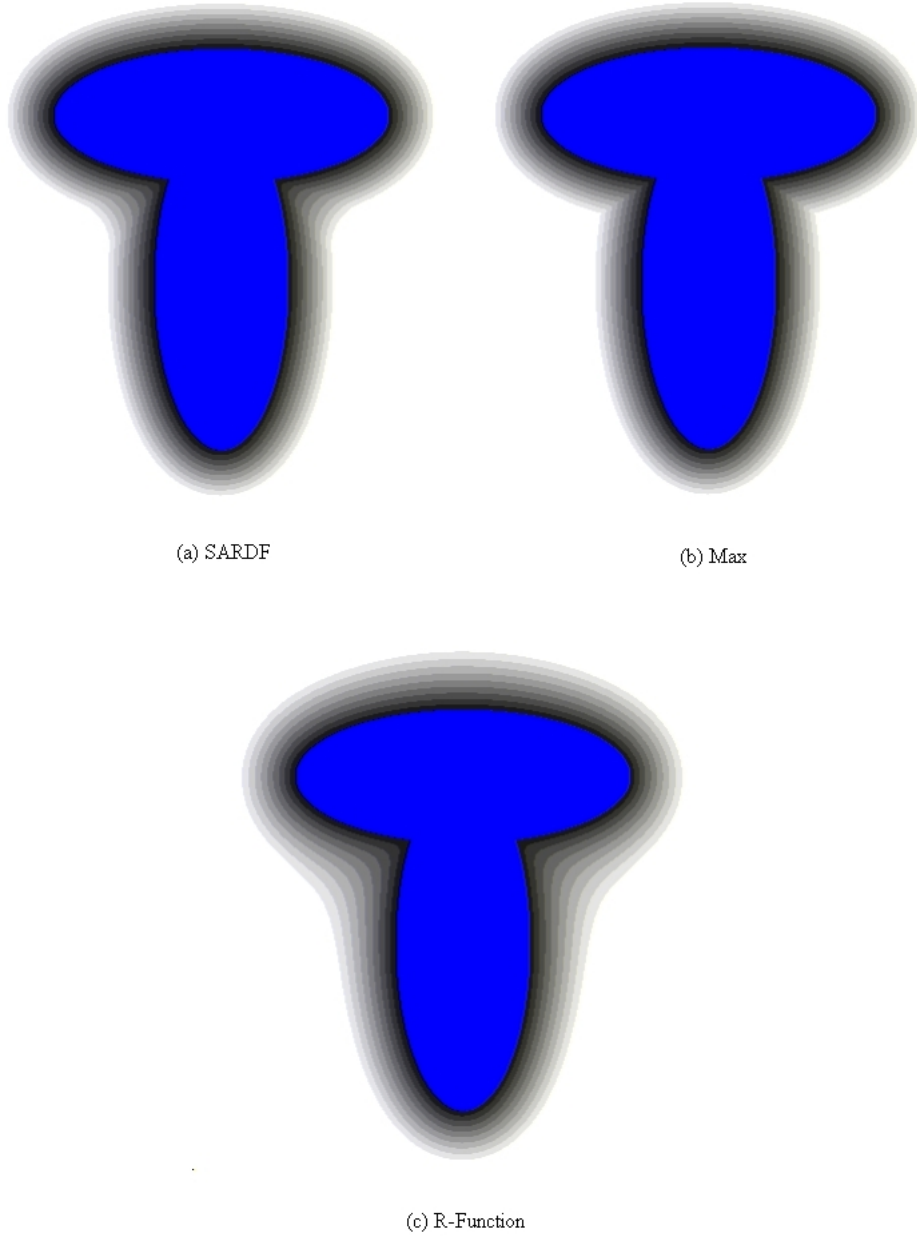
(a) SARDF

(b) Max

(c) R-Function

Figure 15: Union of two ellipsoids with different union operations. The level of gray corresponds to range of distances from points outside the ellipsoid to its surface. (a) SARDF union is used, (b) max is used, (c) R-Function union is used .

in the modeling process preserves a C^1 continuous distance approximation, and makes possible to intuitively model heterogeneous material distributions parameterized by the distance to the material features as proposed in [BST02]. Note that the distance function of normal primitives is not C1 continuous at

the primitives medial axis.

6.1 Two-dimensional CAD part

A simple heterogeneous model is proposed first to illustrate the use of SARDF in constructive heterogeneous object modeling with distance functions. The geometry of the simple CAD part (Fig. 16a) is defined as $f(X) \geq 0$, where f is evaluated by traversing the FRep tree [PASS95] with a box "Box_G", and a cylinder "Cylinder_G" in the leaves (where the G stands for *Geometry*), and the subtraction operation in the node (Fig. 16.b). The box and the cylinder are defined as normal primitives [Har96]. And, the subtraction is defined with SARDF , as follows: $f_1 \setminus_S f_2 = f_1 \wedge_S (-f_2)$.
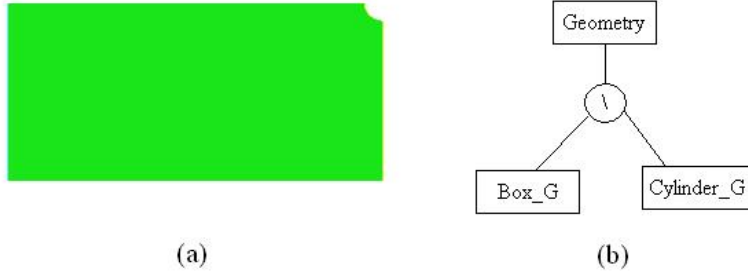

Figure 16: Two-dimensional CAD part. (a) Geometry of the CAD part defined by an FRep. (b) The associated geometric tree, used to define the point set.

This CAD part is constituted of two different materials, with the distribution of each material evolving in space. We use the notation $m_1(X)$ and $m_2(X)$ for the scalar volume fraction component of respectively the materials 1 and 2 in the material composition. For visualization purposes, the material distributions are mapped to the "RGB" color space, i.e. a color is attributed to each material, and the final color is the combination of the colors corresponding to each material, weighted by the scalar volume fraction.

The space partitions SP_1 and SP_2, corresponding to the subspaces, where the two materials are defined, are shown respectively in Fig. 17a and 17b. As for their geometry, the space partitions are defined by building new constructive trees, with SARDF operations in the nodes and normal primitives in the leaves.

Note that the volume fraction component of each material, i.e. $m_1(X)$ and $m_2(X)$, is not constant within the defining space partitions. For example, $m_1(X)$ is constant and equals to 1 only in the subset displayed in Fig. 17c (i.e. the first material feature of the object). In the rest of the space partition, it is a function parameterized by the distance to this material feature shown in Fig. 17c.

In the subset common to both SP_1 and SP_2 (Fig. 17e), the two materials are blended together. The blending is done using the inverse distance weighting [RSST01, She68]. Indeed, in the current example: the scalar volume fraction of each component material are given by: $m_1(X) = w_1(X)M_1$ and $m_2(X) = w_2(X)M_2$, where M_1 and M_2 stands for the value of the scalar volume fraction on the boundary of the first and second material features shown respectively in
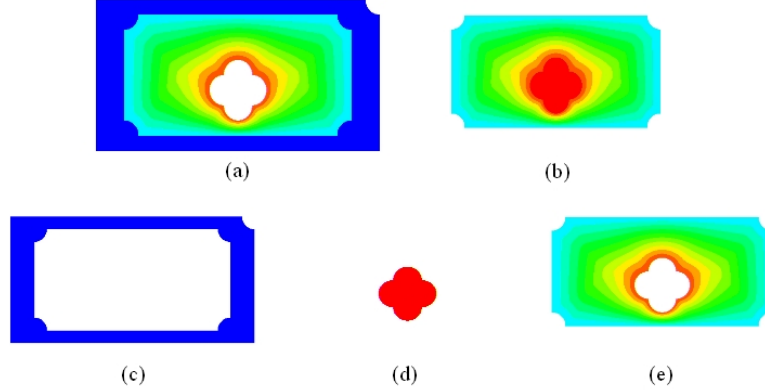
Figure 17: The additional space partitions used to define the materials. (a) The space partition where the material $m_1(X)$ is defined. (b) The space partition where the material $m_2(X)$ is defined. (c) The first material feature, corresponding to the subset where the material 1 is constant $m_1(X) = M_1$. (d) The second material feature, corresponding to the subset where the material 2 is constant $m_2(X) = M_2$. (e) The zone where the materials are blended.

Fig.17c and Fig.17d. In this example, M_1 and M_2 are equal to 1. The weighting functions $w_1(X)$ and $w_2(X)$ are normalization of each inverse distance functions and can be expressed as:

$$w_1(X) = \frac{\frac{1}{d_1(X)}}{\frac{1}{d_1(X)} + \frac{1}{d_2(X)}} = \frac{d_2(X)}{d_1(X) + d_2(X)} \qquad (6)$$

$$w_2(X) = \frac{\frac{1}{d_2(X)}}{\frac{1}{d_1(X)} + \frac{1}{d_2(X)}} = \frac{d_1(X)}{d_1(X) + d_2(X)} \qquad (7)$$

where $d_1(X)$ and $d_2(X)$ are the distances from point X to the boundary of respectively the material features shown Fig. 17c, and Fig. 17d. These two distance maps are also illustrated in Fig. 18 and Fig. 19. Fig. 18a and Fig. 18b correspond respectively to the approximate distance map d_1 when the R-functions and the $SARDF$ operations are used to define the shape. In a similar way, Fig. 19a and Fig. 19b correspond to the approximate distance d_2 when using R-functions and SARDF . The approximate distance maps built using R-functions indicate that even if R-functions have good smoothness properties they are neither exact nor approximate distance functions, making it difficult to control precisely material distribution.

For both weighting functions w_1 and w_2 (see Eq. 6 and 7), two equivalent expressions are given, but the rightmost one should be preferred due to a better numerical stability.

The weighting functions $w_1(X)$ and $w_2(X)$ are continuous functions satisfying the interpolation condition $w_i(\partial B_j) = \delta_{ij}$, where $i, j \in 1, 2$, $\delta_{i,j}$ is the Kronecker symbol[1], and ∂B_j are the boundaries of the material features seen

---

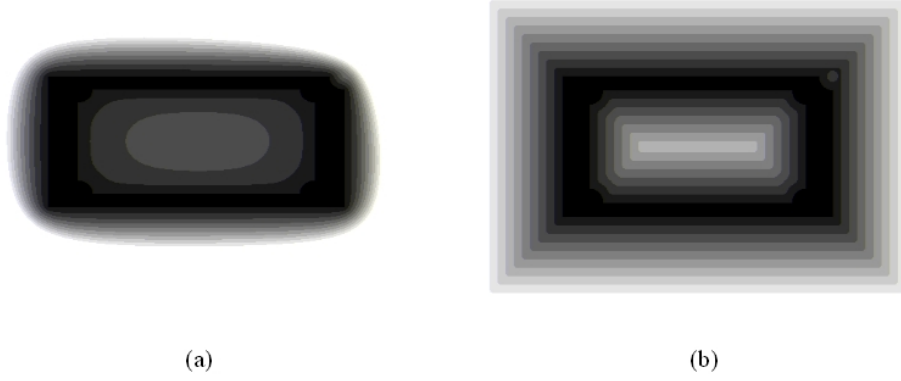[1]equals to 1 if $i = j$ and 0 otherwise

Figure 18: Approximate distance map d_1 from point X to the boundary of the shape Fig. 17c. (a) Using R-functions. (b) Using SARDF operations.
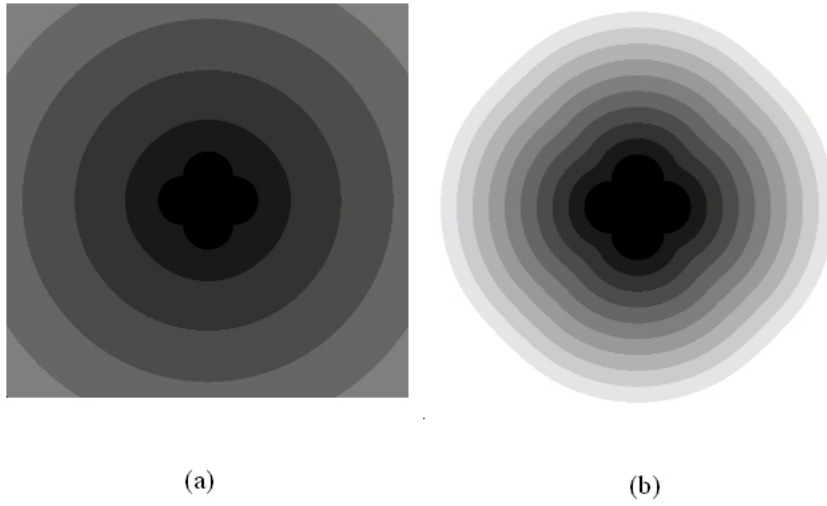

Figure 19: Approximate distance map d_2 from point X to the boundary of the shape Fig. 17d. (a) Using R-functions. (b) Using SARDF operations.

in Fig.17c and 17d. The functions $w_1(X)$ and $w_2(X)$ form a partition of unity.

The mathematical properties of these functions are illustrated in Fig. 20 with a cross section of the model through the $y - axis$ and the visualization of the evolution of the weighting functions $w_1(X' = (x, const))$ and $w_2(X')$ along x-axis. Note that in the current example w_i and m_i, $i \in 1, 2$, have the same graph, since the values of the volume fraction on the boundaries, M_1 and M_2 are equal to 1.
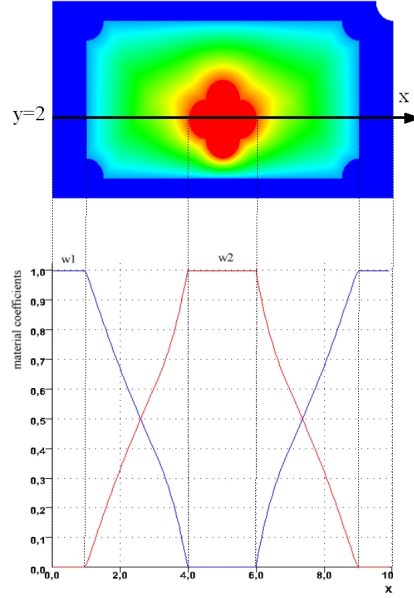

Figure 20: A cross section parallel to x-axis and the distribution of the materials in the cross section.

In the current and following examples only two materials are mixed in the overlapping zone. Of course, more materials can be blended and the expressions for inverse distance weighting (Eq. 6 and 7) can be extended to the case where p materials are blended. Additional details on the inverse distance weighting used for the interpolation of materials defined over functionally defined sets can be found in [RSST01]. More complex expressions for compositions of multiple materials, i.e., vector valued materials, constrained and weighted interpolation of materials, can be found in [BST02].

The resulting model of the CAD part and its material distribution is illustrated by Fig. 21a. The distribution of the material 1, given by its scalar volume fraction $m1(X)$ is mapped to the blue color, and the distribution of the material 2, given by $m2(X)$ to the red color. Stripes are used to make the visualization of the changes in material distribution easier.

Replacing the SARDF operations by R-functions in the constructive trees (both for the geometry and for the space partitions) results in the model shown in Fig. 21b. In general, R-functions have good smoothness (or differential) properties but are neither exact nor even approximate distance functions, see

Fig. 21b, Fig. 18a and Fig. 19a. This results in difficulties for a designer to predict material distribution and to control it.
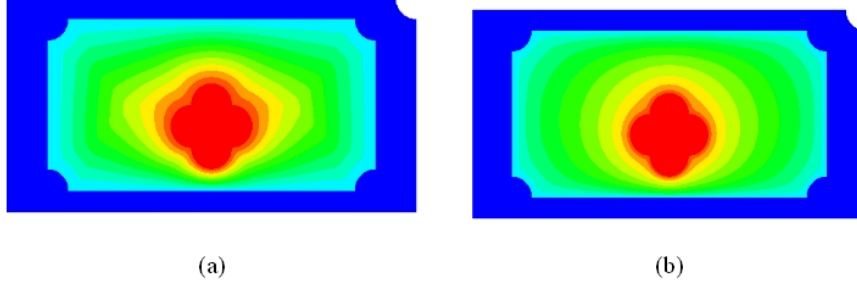

<center>(a)   (b)</center>

Figure 21: Material distribution for the CAD part: (a) with SARDF used for constructive operations; (b) with R-functions used for constructive operations.

6.2 Three-dimensional CAD part

We propose a second example with more complex 3D shapes for the space partitions. The overall geometry of the object is a block. The model includes two attributes; each of them corresponding to the scalar volume fraction of a material. We keep the same notation as in the previous subsection, with $m_1(X)$ and $m_2(X)$ as the scalar volume fraction of the materials 1 and 2.

The domains of definition of each attributes, i.e. their space partitions, are shown Fig. 22a for the first material and Fig. 22b for the second material. These space partitions are respectively named SP_1 and SP_2.
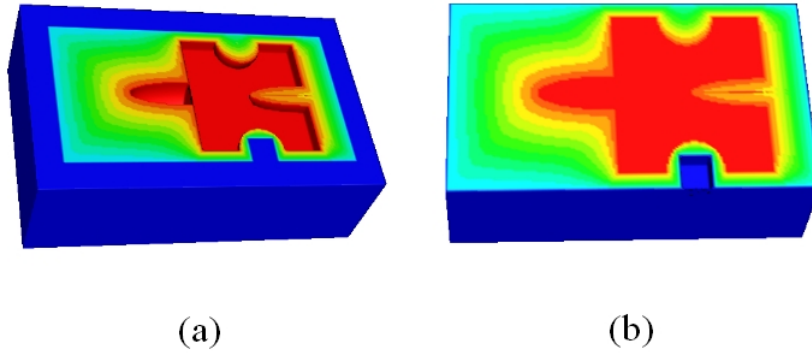

<center>(a)   (b)</center>

Figure 22: The two space partitions for the heterogeneous model: (a) the first space partitions SP_1, corresponding to the first attribute, (b) the second space partition SP_2, corresponding to the second attribute.

The object contains two material features: Fig. 23a shows the first material feature corresponding to $X \in SP_1 : m_1(X) = M_1 = 1$ cut by a planar half-space for visualization purposes only. Figure 23b shows the second material feature corresponding to $X \in SP_2 : m_2(X) = M_2 = 1$; the geometry of this latter space

partition is composed only of blocks and ellipsoids, combined with SARDF unions and intersections. Figure 23b shows a zoom to one of the pins. Such a pin is modeled only with ellipsoids as primitives and SARDF union and intersection as operations. Indeed, it is the SARDF union of four ellipsoids, that are after subtracted from a fifth ellipsoid.
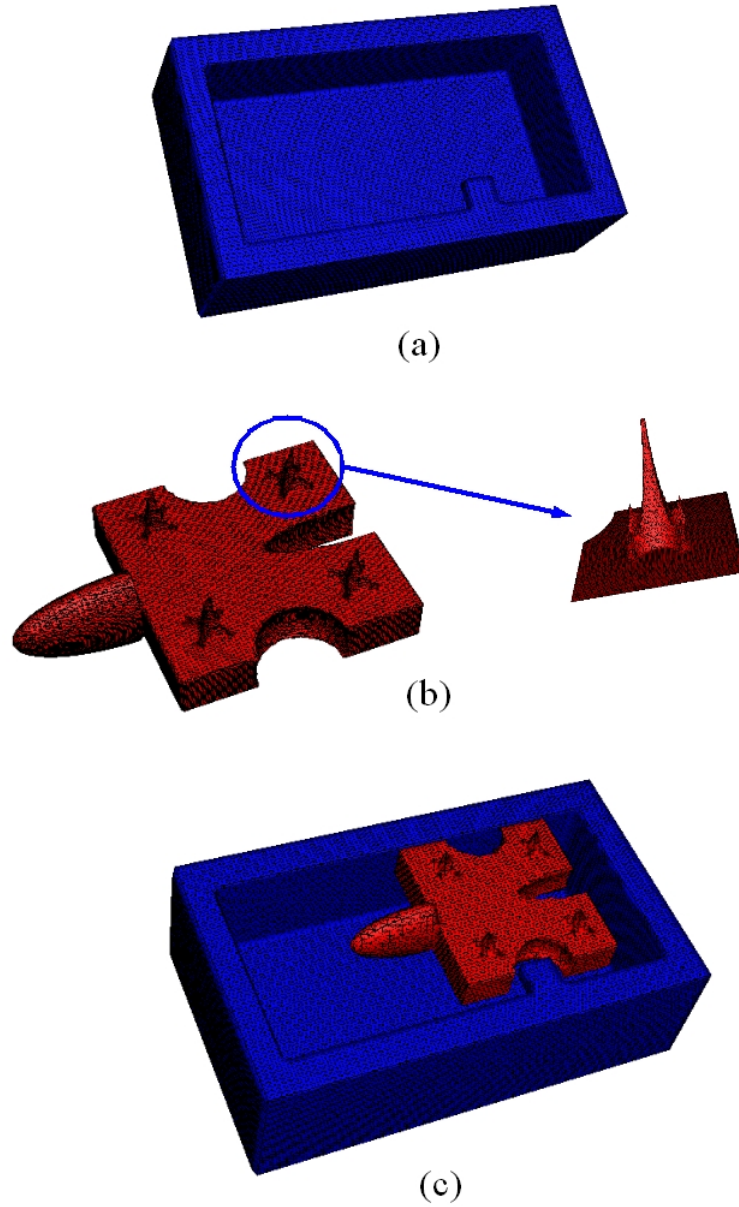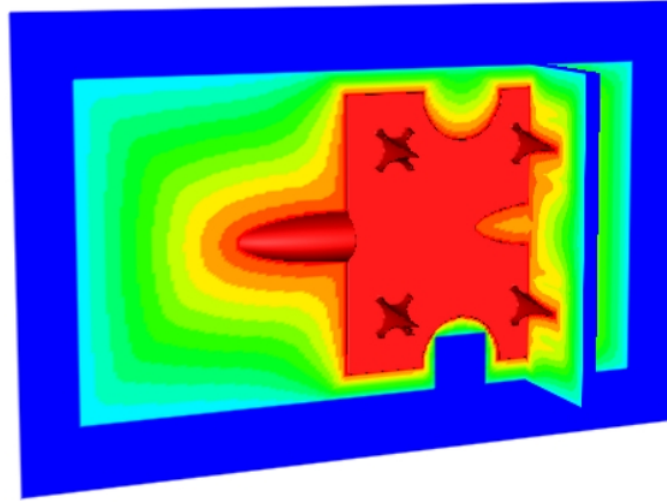

Figure 23: (a) the first material feature, (b) the second material feature, with a zoom on one of the pins, on the right, (c) union of the two material features.

For this model, the two space partitions are intersecting: the common space
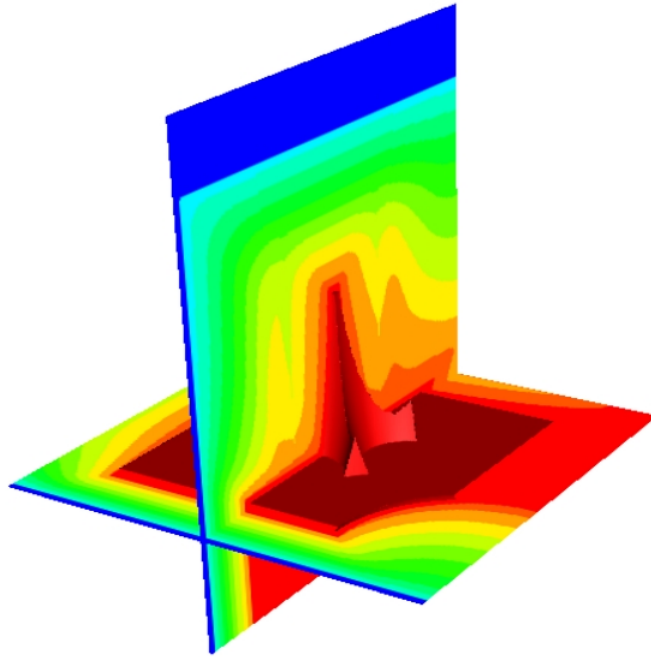
29

can be seen Fig. 22 with the gradient of colors. In this common space, the two materials are blended together. The blend is done by the same technique as used in 6.1. The expression for each coefficient is the same as in section 6.1, Eq. 6 and Eq. 7.

The overall distribution of the materials is shown Fig. 24a. The geometry corresponding to the second material feature is rendered, using a red color, then for the visualization of the material distribution, two cross-sections are made: one for $x = 0$ and one for $z = 0$. On each of the cross-section, the evolution of the material distribution is projected. For visualization purposes, each material is mapped to one color. The first material corresponds to the blue color and the second material to the red.

Figure 24b shows a zoom to one of the pins. The space where the coefficient of the material m_2 is equal to one, is drawn in 3D with red color. Two more cross sections with distribution of materials are added. Red color is associated with the second material, and blue color with the first material. The gradient of color expresses the evolution of the distribution of the material composition, indicating percentage of the first and second material.

Figure 24: Distribution of two materials. Blue color corresponds to material 1, red color to material 2. The color variation indicates the fraction of each material. (a)Two cross sections are made for $x = 0$ and $y = 0$ to show the material distribution. (b) A zoom is made to one of the pins with additional cross-sections.

6.3 Tooth inlay

An image of a real tooth is shown in Fig. 25. Contours have been hand drawn for the outside shape, the inlay, and the middle contour, mixed zone with tooth and inlay material. The distance between the inlay and the middle contour is taken bigger than in reality just for presentation purposes.

Figure 25: Image of a real tooth with the inlay and with hand drawn contours: outside shape, middle contour and inlay.

The hand drawn contours are approximated by polylines first and then converted to the function representation using the algorithm proposed in [Rva74] and described in [PSS96] with the R-functions replaced by the corresponding SARDF . The corresponding shapes are displayed in Fig. 26a for the outside tooth shape, Fig. 26b for the inlay, and Fig. 26c for the middle contour.

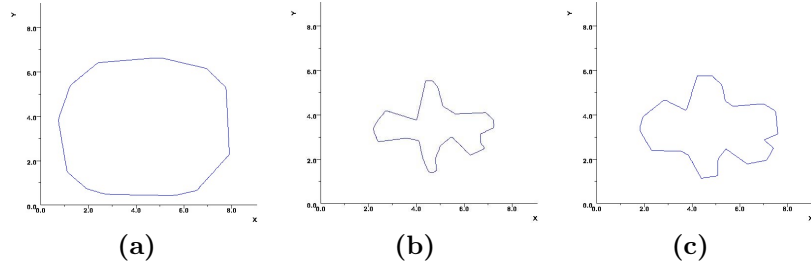|		
(a)	(b)	(c)

Figure 26: FRep model of the tooth with the inlay: (a) the outside tooth shape; (b) the inlay; (c) the middle contour.

Two space partitions are defined on the geometric shape shown in Fig. 26a; the first partition, SP_1, is defined by the subtraction of the inlay from the outside tooth shape; the second partition, SP_2, is defined by the middle contour itself.

The model contains two material features: the first one corresponds to the zone of pure material tooth (in light red Fig. 25). The second material feature corresponds to the pure inlay material (see in black Fig. 25).

Two attributes are used in the model: the first one is defined on SP_1, and corresponds to the tooth material; the second one is defined on SP_2, and corresponds to the inlay material. The final heterogeneous object is defined by the triplet: (outside tooth shape, tooth material, inlay material).

Two space partitions SP_1 and SP_2 are overlapping in the area corresponding to the subtraction of the inlay (Fig. 26b) from the middle space (Fig. 26c). In this common space, the two materials are blended. The volume fraction of each component material is constructed in this overlapping space, by weighting the volume fraction in each material feature. The weighting coefficients are defined by the inverse distance weighting following equations Eq. 6 and Eq. 7.

The distribution of the materials is visualized by mapping them to the "RGB" color space. Figure 27a is a rendered image of the tooth inlay material (dark color) using a radius of 0.5 for the SARDF functions. For comparison purposes, the tooth inlay is also modeled with R-Functions (Fig. 27b) in both of the constructive trees: for the geometry and the space partitions. The latter figure stresses again the difficulties to model complex heterogeneous objects with R-Functions, because of the incorrectness of the distance function approximation.
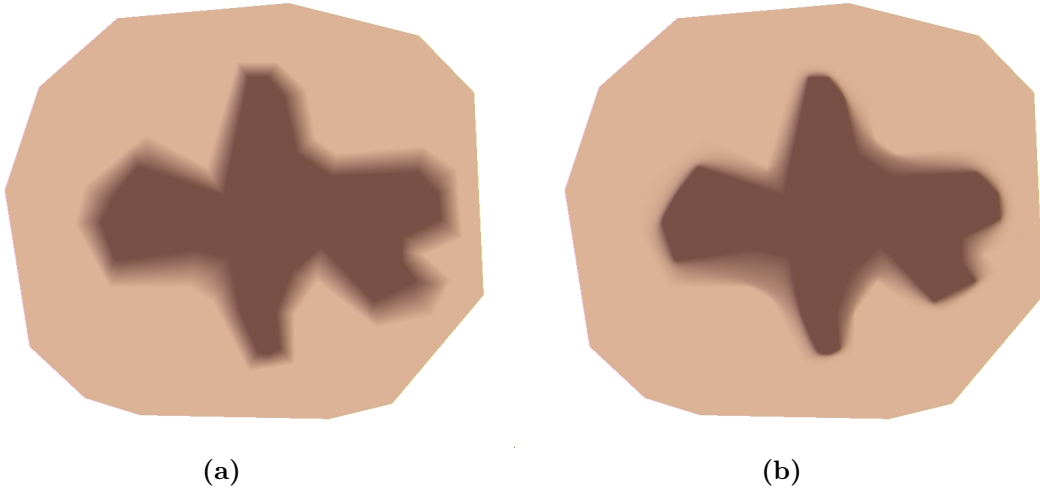

(a)   (b)

Figure 27: (a) Rendering of the tooth inlay with a radius of 0.5; (b) Same as picture (a) but R-functions have been used in the constructive trees for the geometry and the space partitions.

For ease of visualization, the material distribution is drawn in Fig. 27a, using stripes. The result is shown on Fig. 28; a zoom is done to the circled region and shown in Fig. 29a, where SARDF operations are used, and Fig. 29b for R-Functions.

Both material distributions along the x-axis for a cross section in $y = 2$ are drawn in Fig. 30. The topmost picture corresponds to the geometric space, with the contours of the space partitions within. A black horizontal line, drawn for $y = 2$, indicates where the cross-section is done. The middle and bottom pictures are graphs illustrating the fractions of each material, the middle one corresponds to the distribution of the first material (tooth material) along x-axis, and the bottom corresponds to the distribution of the second material (tooth inlay).
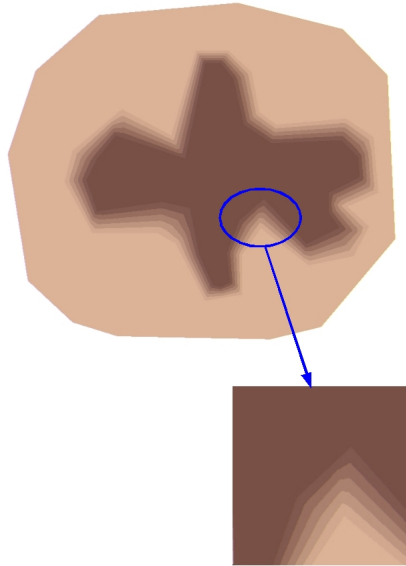
Figure 28: A lookup table is used to produce stripes to show the material distribution. The circled zone is zoomed and shown below.
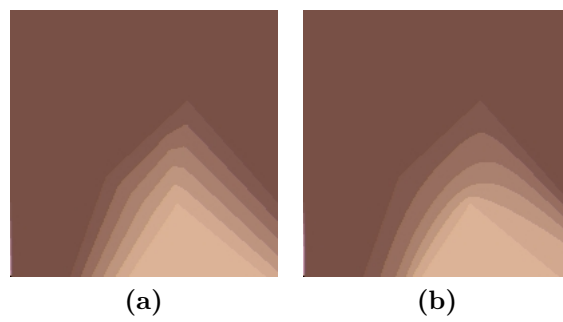

(a)   (b)

Figure 29: Comparison of SARDF and R-functions for the zoom shown in Fig. 28. (a) SARDF are used; (c) R-functions are used.
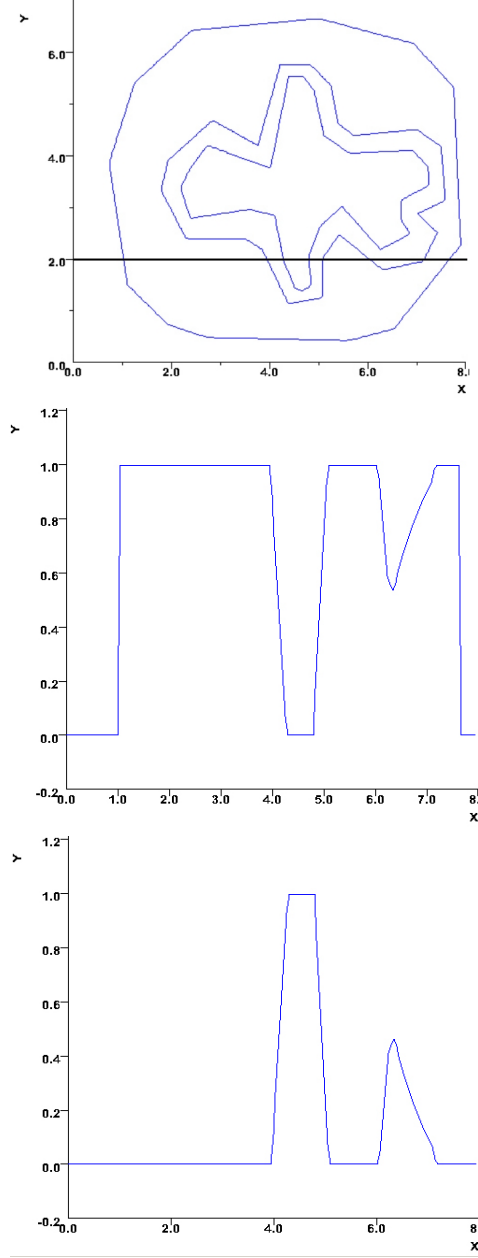
Figure 30: Material distributions for the tooth with the inlay: (top) geometric shape and space partitions; (middle) evolution of the fraction of the tooth material along x-axis (cross section for $y = 2$); (bottom) evolution of the fraction of the inlay material along x-axis.

35

7 Conclusion

In this paper, we studied the issues of heterogeneous object modeling, especially the control of the distribution of given materials inside an object. The constructive hypervolume model [PASS01] serves as a basis for our work. We put constraints on this model for the special purpose of heterogeneous objects modeling following the idea of [BST02] stating that the distribution of a material can be precisely modeled and controlled using distances to some material features (shape subsets where the property of the material is known).

The core of this work is the introduction and application of special functions describing set-theoretic operations for constructive modeling. Under the condition that the primitives in use are defined by exact distance functions, the proposed set of functions provides for a good approximation of the real distance value. Furthermore, the upper limit of the error in the distance computation can be exactly determined. These functions serve for defining both the object geometry and the space partitions where the materials are defined.

The proposed operations are first defined for two half planes as $x \geq 0$ and $y \geq 0$ in each quadrant of a two dimensional space. While in quadrant II and IV, they are exactly equal to min, max; in quadrants I and III, a circular approximation of min, max is used with an additional bounding band limiting the growth of the distance function error.

The result of any constructive modeling, involving signed approximate real distance functions (SARDF) and primitives defined by distance functions, is at least C^1 continuous, except for the cases when both of the arguments of the SARDF operation are equal to 0, or for the points belonging to the medial axis of one of the primitives. The investigation of some analytical expressions for primitives, that approximate distance function, but avoid the C^1 discontinuity on the medial axis, is a source of future work.

Through the case studies, the viability of the proposed functions for constructive heterogeneous modeling is confirmed. The provided examples can be easily extended with more complex material distribution for the material features and more complex scheme for combination of the different attributes, since no restrictions prevent it in our model.

References

[AKK+02] V. Adzhiev, E. Kartasheva, T. Kunii, A. Pasko, and B. Schmitt. Hybrid cellular-functional modeling of heterogeneous objects. *Journal of Computing and Information Science in Engineering, Transactions of the ASME*, 2(4):312–322, December 2002.

[BDS+03] L. Barthe, N. A. Dodgson, M. A. Sabin, B. Wyvill, and V. Gaildrat. Two-dimensional potential fields for advanced implicit modeling operators. *Computer Graphics Forum*, 22(1):23–33, 2003.

[BS01] A. Biswas and V. Shapiro. Approximate distance fields with nonvanishing gradients. Technical report, University of Wisconsin-Madison, 2001.

[BSD00] S. Bhashyam, K.H. Shin, and D. Dutta. An integrated cad system for design of heterogeneous objects. *Rapid Prototyping Journal*, 2000.

[BST02] A. Biswas, V. Shapiro, and I. Tsukanov. Heterogeneous material modeling with distance fields. Technical report, University of Wisconsin-Madison, 2002.

[CF03] K. Chen and X. Feng. Computer-aided design method for the components made of heterogeneous materials. *Computer-Aided Design*, 2003.

[CT00] M. Chen and J. Tucker. Constructive volume geometry. *Computer Graphics Forum*, 19(4):281–293, 2000.

[FPS03] P.A. Fayolle, A.A. Pasko, and B. Schmitt. Distance function approximation for constructive shape modeling. Technical Report TR 2003-1-06, University of Aizu, Tsuruga, Ikki-machi, Aizu-Wakamatsu City, Fukushima, 965-8580 Japan, November 2003.

[Har94] John C. Hart. Distance to an ellipsoid. In Paul Heckbert, editor, *Graphics Gems IV*, pages 113–119. Academic Press, Boston, 1994.

[Har96] J. Hart. Sphere tracing: A geometric method for the antialiased ray tracing of implicit surfaces. *The Visual Computer*, 12(10):527–545, 1996.

[KBDH99] V. Kumar, D. Burns, D. Dutta, and C. Hoffman. A framework for object modeling. *Computer-Aided Design*, 31(9):541–546, 1999.

[KD97] V. Kumar and D. Dutta. An approach to modeling multi-material objects. pages 336–345, 1997. Fourth Symposium on Solid Modeling and Applications.

[Nie00] G. Nielson. Volume modelling. *Volume Graphics, M. Chen, A. Kaufman, R. Yagel (Eds.), Springer-Verlag*, pages 29–48, 2000.

[PASS95] A. Pasko, V. Adzhiev, A. Sourin, and V. Savchenko. Function representation in geometric modeling: concept, implementation and applications. *The Visual Computer*, 1995.

[PASS01]   A. Pasko, V. Adzhiev, B. Schmitt, and C. Schlick. Constructive hypervolume modeling. *Graphical Models*, 2001.

[PSS96]   A.A. Pasko, A.V. Savchenko, and V.V. Savchenko. Implicit curved polygons. Technical Report 96-1-004, University of Aizu, Japan, 1996.

[QD01]   X. Qian and D. Dutta. Physics based b-spline heterogeneous object modeling. In *DETC and Computers and Information in Engineering Conference*. ASME, September 2001.

[Req80]   A. Requicha. Representations for rigid solids: theory, methods, and systems. *ACM Computing Surveys*, 12(4):437–464, 1980.

[Ric73]   A. Ricci. A constructive geometry for computer graphics. *The Computer Journal*, 16(2):157160, 1973.

[RSST01]   V.L. Rvachev, T.I. Sheiko, V. Shapiro, and I. Tsukanov. Transfinite interpolation over implicitly defined sets. *Computer Aided Geometric Design*, 2001.

[Rva63]   V. Rvachev. On the analytical description of some geometric objects. Technical Report 4, Ukrainian Academy of Sciences, 1963.

[Rva74]   V. Rvachev. Methods of logic algebra in mathematical physics. Technical report, Naukova Dumka, 1974.

[Rva82]   V. Rvachev. Theory of r-functions and some applications. Technical report, Naukova Dumka, 1982.

[Sab68]   M. Sabin. The use of potential surfaces for numerical geometry. Technical report, British Aircraft Corporation, 1968.

[She68]   D. Shepard. A two-dimensional interpolation function for irregularly spaced data. Number 23, pages 517–524, 1968. Proceeding 23 National Conference.

[SPAS01]   B. Schmitt, A. Pasko, V. Adzhiev, and C. Schlick. Constructive texturing based on hypervolume modeling. *Journal of Visualization and Computer Animation*, 12(5):297–310, 2001. http://www3.interscience.wiley.com/cgi-bin/abstract/94518525/START.